Flow patterns and mass transfer performance of miscible liquid-liquid flows in various microchannels: Numerical and experimental studies

Jenifer Gómez-Pastora, Cristina González-Fernández, Marcos Fallanza, Eugenio Bringas, Inmaculada Ortiz

PII: S1385-8947(18)30468-6
DOI: https://doi.org/10.1016/j.cej.2018.03.110
Reference: CEJ 18717

To appear in: *Chemical Engineering Journal*

Received Date: 24 October 2017
Revised Date: 19 March 2018
Accepted Date: 21 March 2018

Please cite this article as: J. Gómez-Pastora, C. González-Fernández, M. Fallanza, E. Bringas, I. Ortiz, Flow patterns and mass transfer performance of miscible liquid-liquid flows in various microchannels: Numerical and experimental studies, *Chemical Engineering Journal* (2018), doi: https://doi.org/10.1016/j.cej.2018.03.110

Flow patterns and mass transfer performance of miscible liquid-liquid flows in various microchannels: Numerical and experimental studies

Jenifer Gómez-Pastora, Cristina González-Fernández, Marcos Fallanza, Eugenio Bringas and Inmaculada Ortiz*

Dept. of Chemical and Biomolecular Engineering, ETSIIT, University of Cantabria, Avda. Los Castros s/n, 39005 Santander, Spain

*Correspondence to: Dept. Chemical and Biomolecular Engineering, ETSIIT, University of Cantabria, Avda Los Castros s/n, 39005 Santander, Spain.

E-mail: ortizi@unican.es; Phone: +34 942201585; Fax: +34 942201591

ABSTRACT

The advantages of miniaturized systems and the laminar flow regime that is present in microfluidic channels have opened a new range of applications in which the use of multiple streams with different reagents is exploited. However, further development of these microdevices needs deeper understanding on the phenomena involved in order to efficiently design such microsystems. In this work, we report the analysis of the solute mass transport performance in Y-Y-shaped microchannels as a function of the couple influence of both the flow patterns and mass transport kinetics. With this objective, the influence of the following operation variables has been analyzed, the ratio between the residence and diffusion times (γ) and the volumetric ratio between the fluid phases (α), that was determined for three different geometric configurations. The performance of the devices was presented as the solute separation factor in the donor fluid and the concentration factor in the receiving phase. Results showed that the ratio α greatly impacts the solute concentration value reported in both phases for the same γ value, which in turn influences the solute mass flow at the channel outlets. Both the flow patterns and the concentration gradients developed inside the systems were numerically studied by using Computational Fluid Dynamics (CFD) techniques and experimentally analyzed by fluorescence microscopy with fluorescein employed as model solute. This study represents a thorough analysis of the phenomena that determine the performance of the separation of solutes between homogeneous flowing fluids in microdevices where the fluid dynamics are coupled with mass transfer phenomena and facilitates its extension to the general case where separation is enhanced by chemical reactions.

Keywords: Microfluidics, multiphase flow, miscible fluids, phase separation, diffusion, mass transfer.

1. INTRODUCTION

Within the last decade, the use of microdevices has attracted great attention inside the scientific community for analytical, chemical or biomedical processes [1-4]. The miniaturization of these processes provides many advantages because, in addition to its high surface area to volume ratio, which varies from 10,000 to 50,000 m^2/m^3 [5], microfluidics allows an exhaustive control of the fluid dynamics. It also offers enhanced mass and heat transfer rates, so these devices can be used to carry out mass-transfer-limited processes or highly exothermic reactions where a better temperature control and thus suppression of hot spots could be desired [6]. Moreover, since small sample volumes are required, risks involved in handling hazardous materials are minimized and the use of expensive reagents for experimental analyses can be spared [7]. Therefore, microfluidics has been considered as a promising technology that covers two main frameworks: i) process intensification with an improvement of safety, including the development of highly efficient industrial processes (i.e. the factory-on-chip concept, as recently reported by Han et al. [8]), and ii) lab on a chip (LOC) devices explored for rapid data acquisition at laboratory scale, including kinetics, physico-chemical properties and biological information, which could guide the proper design of traditional pilot and industrial plants [9,10].

As a result, microfluidics has been rapidly expanded to carry out small-scale chemical, biochemical, and pharmaceutical processes involving single or multiphase flows [11-14]. In fact, an important advantage of the laminar flow that is present within microfluidic channels is that when multiple liquids are employed, they flow side-by-side in a highly stable manner; thus, mixing between adjacent streams occurs only by diffusion [15,16]. Due to the traditional concept of interface, usually recognized as the common boundary between immiscible fluids, a great number of studies has been carried out to understand the flow regimes of immiscible liquid-

liquid systems in microchannels [17-20]. However, if fluids are miscible apparently this interface does not exist but still, two miscible fluids, usually liquids, brought into contact will have a boundary between them that disappears as the fluids start mixing [21]. This boundary region in fact acts as a real interface between both liquids, sharing most of its properties with those of the interface between immiscible fluids [22]. Therefore, if two miscible liquids flow next to each other under laminar flow conditions, it would be possible to control their diffusive interface [23]. The precise control that microfluidics offers over the flowing conditions and the shape and location of the interface, enables the separation of miscible phases brought in contact under stratified flow conditions. This has opened a new range of applications that were not previously possible [2,6,11,14,16]. For all these applications, it is critical to possess deep understanding of the fluid dynamics of the flowing fluids as well as mass transfer kinetics of the solutes contained in the fluids.

Regarding the co-flow of two miscible phases, it is well-known that fluids with the same properties should flow at the same volumetric flow rate in Y-Y shaped symmetric devices (i.e. devices where the volumetric fraction occupied by the fluids is the same) in order to achieve complete phase separation at the outlets. However, no studies have been carried out to determine the conditions that achieve the separation of co-flow phases in asymmetric devices where different volumetric ratios between the fluids are employed, although these devices are useful for different processes [24]. Furthermore, it has been also demonstrated that fluids with different properties (especially, different viscosities), at the same volumetric flow rate are not completely separated at the outlets of symmetric channels because the interface between the two streams is not located at the channel midline [25-27], and as a result, different approaches have been used

to achieve phase separation [7], some of them based on trial-and-error experimental procedures [28,29].

Studies focused on the molecular diffusion of solutes between colaminar streams in symmetric channels are abundant [23,25,26,30-32]. It has been considered that the solute will be transferred between co-flowing solutions if the residence time is higher than the diffusion time for the solute to diffuse between fluids [33,34]. Therefore, the diffusion length H (considered equal to the height of the branch in which the solution with the solute flows) plays an important role, as the diffusion time is proportional to H^2 [7]. However, analysis regarding the concentration gradients when H varies but the total height of the channel is kept fixed (various channel designs) are lacking, although different investigations have demonstrated that the microchannel geometrical characteristics affect the mass transfer performance between immiscible fluids [9,35-39].

The objective of this article is to deepen in the analysis of the hydrodynamics and mass transfer between homogeneous phases inside microchannels; the methodology is based on the study (theoretical and experimental) of the coupled influence of fluid dynamics and mass transfer on the separation of a solute. In this work, we selected different Y-Y shaped channels that specifically involve different volumetric ratios between the fluid phases. Theoretical analyses have been carried out by Computational Fluid Dynamics (CFD) techniques. Firstly, the flow patterns of two miscible fluids are studied in both symmetric and asymmetric channels and the conditions that lead to the complete phase separation are analyzed. Secondly, the diffusion of fluorescein as model compound is studied as a function of the ratio between the residence and diffusion times for different geometries. Good agreement between the experimental and numerical results was found, verifying the ability of the CFD model to predict the concentration gradients developed inside Y-Y shaped channels for a wide range of flow rates. Thus, this design

methodology should prove useful in determining the optimum flow rates and geometry configuration for applications that involve confined flow of different homogeneous phases.

2. MATERIALS AND METHODS

2.1. Theory

In this section, a mathematical model able to predict the flow field developed by 2 miscible phases and the diffusion of a component between fluids inside asymmetric and symmetric microdevices is derived. The plane x-z of the microchannels employed in the simulations is schematized in Fig. 1. The solute (fluorescein) is transferred from an aqueous solution (Phase 1) to deionized water (Phase 2).

General microfluidic devices usually involve the use of channels with width dimensions around 100 micrometers and several millimeters in length [11]. These values were taken as reference and we designed different channel geometries with a total width of 200 μm and 2 mm in length (1/10 aspect ratio between width and length) as seen in Fig. 1. Thus, for the symmetric device (Fig. 1 a)), the channel heights (H_1 and H_2) were set at 100 μm and the length (L) was 2 mm. Therefore, the volumetric ratio between the fluids ($\alpha=V_1/V_2$) is equal to 1. For the asymmetric channels, the same geometry was employed but the phases were fed through different inlets as seen in Figs. 1 b) and c). In these cases, H_1 and H_2 were modified and took the values of 40 and 160 μm for the configuration 1 (Fig. 1 b)), and 160 and 40 μm for the configuration 2 (Fig. 1 c)), which is translated into α ratios equal to 0.25 and 4, respectively.

The theoretical model basically involves a CFD-based Eulerian approach, where the fluid flow is predicted by solving the Navier-Stokes equations under laminar flow conditions and the diffusion of a compound is modelled by inserting the Fick's law into the continuity equation for

that component. These equations are numerically solved using the Volume of Fluid (VOF) method. The fluids are considered to be incompressible and Newtonian.

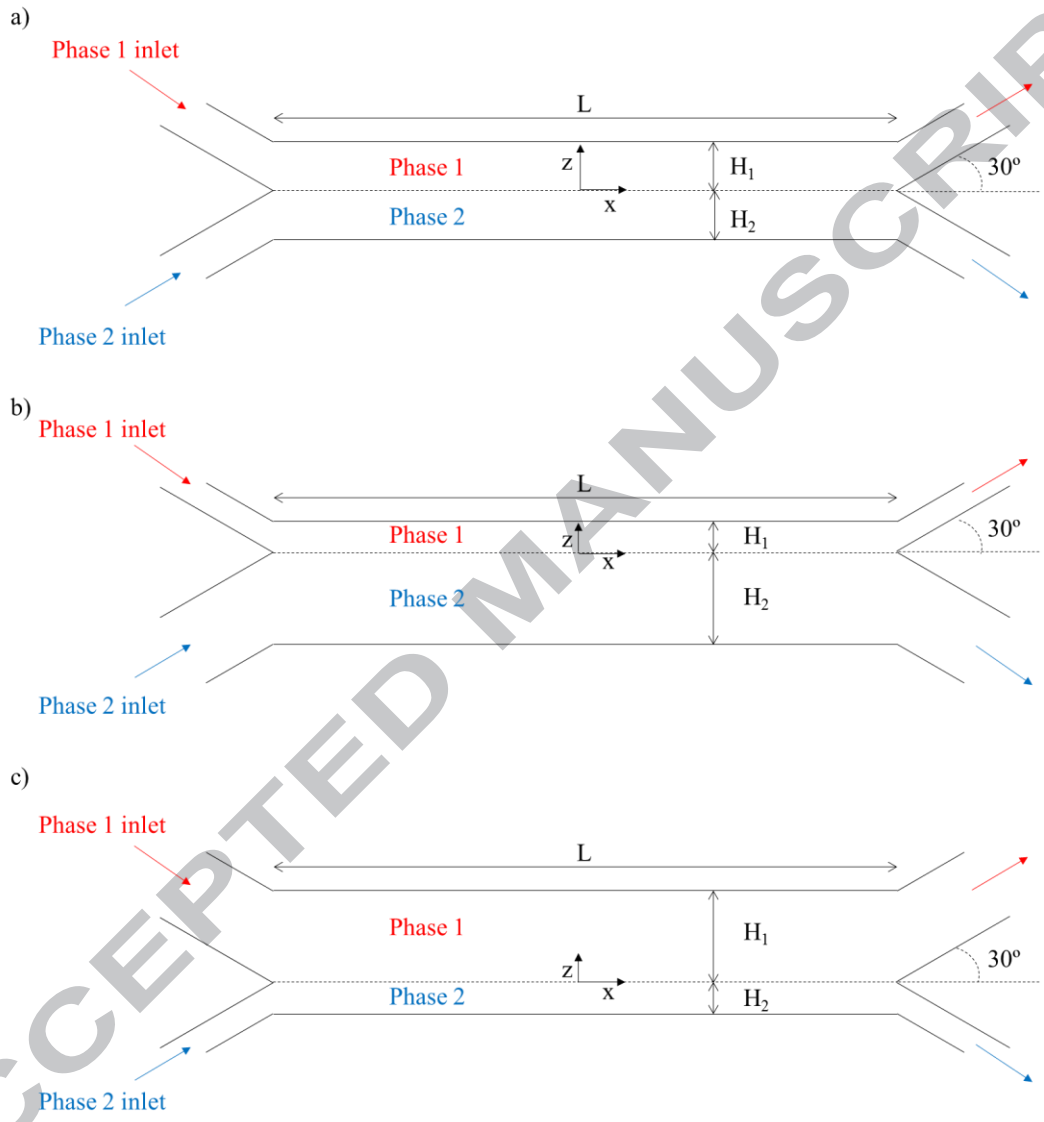

Fig. 1. Microfluidic devices employed in this work. a) Symmetric configuration; b) Asymmetric device with configuration 1; c) Asymmetric device with configuration 2.

Fluid configurations are defined in terms of a VOF function, F, that satisfies the following equation under laminar conditions:

$$\frac{\partial F}{\partial t} + \frac{1}{V_F}[\nabla(F\mathbf{A}\mathbf{v})] = 0 \quad (1)$$

where V_F and $\mathbf{A}$ represent the fractional volume and fractional area open to flow for each mesh cell, and $\mathbf{v}$ the fluid velocity. Thus, the VOF function, F, represents the volumetric fraction of the incompressible phase 1 and the complementary region with volumetric fraction 1-F, represents the volumetric fraction of the other fluid in every computational mesh cell (phase 2). It should be noted that Eq. (1) must be modified under certain circumstances (e.g. modeling of shock waves, chemical reactions, etc.) [40].

The fluid velocity field is governed by the mass continuity and momentum equations, which are solved under the assumption that the fluids are incompressible, i.e.:

$$\frac{\partial \mathbf{v}}{\partial t} + \frac{1}{V_F}(\mathbf{v}\mathbf{A}\nabla\mathbf{v}) = -\frac{\nabla P}{\rho} + \mathbf{f} \quad (2)$$

$$\nabla \cdot (\mathbf{v}\mathbf{A}) = 0 \quad (3)$$

where P is the pressure and $\mathbf{f}$ represents the viscous accelerations. Eqs. (2) and (3) within the VOF method are solved by using a volume-fraction-weighted density (ρ) and viscosity (μ) through the function F. Since in this work we employ the same fluid for both phases, the density and viscosity values for the mixture (i.e. when the mesh cell is being occupied by both fluid phases ($0 \leq F \leq 1$), as for example in the interface cells) are the same as those reported by the isolated fluid phases. However, this method can be perfectly extended to different fluids, i.e. when the properties of the phases are not the same.

In addition to the flow parameters described above, the model also solves the mass transport of species between both phases by solving the continuity equation and the Fick's law. The presence

of a solute is defined as a property of both fluids (advectable scalar) and it is treated as an interstitial solute, i.e. the molecules fit perfectly in the spaces between the molecules of the solvent. The advectable scalar in this work is defined as the concentration C in terms of mass per fluid volume in cell. The transport equation that is calculated for the advectable scalar is given as follows:

$$\frac{\partial C}{\partial t} + \frac{1}{V_F}(\mathbf{v}\mathbf{A}\nabla C) = \frac{1}{V_F}[\nabla(\mathbf{A}D\nabla C)] \quad (4)$$

in which D is the solute's diffusion coefficient, which takes the value of $4.25 \cdot 10^{-6}$ $cm^2 \cdot s^{-1}$ in this work. The presence of dissolved species does not affect the fluid dynamics since they move with the mean flow (they can only increase the fluid density).

It should be noted that when contacting several fluid phases at different velocity values, there is a momentum transfer between them at the interface that affects the velocity field; however, solute transport in the direction normal to the flow only occurs due to a concentration gradient as presented in Eq. (4). Furthermore, if the fluids to be contacted at the microchannel were different showing an interfacial distribution ratio of the solute (solubility), or if there were a chemical reaction taking place at the interface (e.g. microextraction processes with an organic solvent), these additional phenomena should be included in the model. Moreover, for those cases where two different fluids were contacted inside the device, different diffusion coefficients should be included for solving Eq. (4).

In this work, we analyze the component diffusion between phases through the interface as they flow within the channel according to the component's diffusion time. This time represents the time required for partitioning of solutes between the phases and is proportional to $\frac{H_i^2}{jD}$, where H_i is the height of the channel where the phase "i" is flowing through, "j" represents the number of

dimensions in which diffusion takes place and D represents the diffusion coefficient of the component [41]. Thus, if the residence time exceeds the diffusion time of the solute inside the device, the model component will have enough time to diffuse to the co-flowing phase. Therefore, we study the diffusion at different values of the ratio γ (between 0.1 and 4), described as follows:

$$\gamma = \frac{\text{Residence time}}{\text{Diffusion time}} = \frac{\frac{L}{\overline{v_1}}}{\frac{H_1^2}{jD_{fluorescein}}} \quad (5)$$

where L represents the chip total length (2 mm) and $\overline{v_1}$ the average velocity of phase 1 (inlet velocity), whereas H_1 is the height of the branch where phase 1 flows and $D_{fluorescein}$ the diffusion coefficient for the fluorescein, $4.25 \cdot 10^{-6}$ $cm^2 \cdot s^{-1}$ [42]. Since the diffusion time is fixed for each geometry, the analysis corresponding to different γ values was conducted by changing the average inlet velocity value for the fluorescein phase, leading to different values of the residence time. Although the axial velocity inside the channel gradually changes from zero at the walls to a maximum value in the center [43], the average residence time was taken than the residence time distribution along the channel height, which would render a more complex analysis and result impractical for real applications.

Furthermore, the results of the diffusion analysis under steady state conditions are presented through two dimensionless numbers, the separation factor in the donor phase and the concentration factor in the receiving phase, described as follows:

$$\text{Separation factor} = \frac{(C_{1,x=-L/2} - C_{1,x=L/2})}{C_{1,x=-L/2}} \quad (6)$$

$$\text{Concentration factor} = \frac{C_{2,x=L/2}}{C_{1,x=-L/2}} \quad (7)$$

where $C_{1,x=-L/2}$ and $C_{1,x=L/2}$ represent the initial and final concentration of fluorescein in phase 1 (at x=-L/2 and x=L/2, respectively), and $C_{2,x=L/2}$ is the final concentration found at the outlet in phase 2. Thus, the separation factor is related to the transport of the solute by diffusion from phase 1 (dilution effect), and the concentration factor represents the final concentration of fluorescein in phase 2 compared to the initial concentration in phase 1. Additionally, the mass flow of fluorescein (product between the concentration and the volumetric flowrate) for each phase at the outlets was calculated.

All the equations were solved using the commercial flow solver ***FLOW-3D*** v11 (Flow Science, Inc.). Water properties at 20ºC were used to model both fluids 1 and 2 (ρ=1000 kg·m^{-3}, μ=0.001 Pa·s) and fluorescein sodium salt was selected as model compound to formulate solutions with initial concentrations of about 60 mg·L^{-1} that were fed into the microdevices through the upper inlet (Phase 1).

Finally, a mesh independence study was carried out in order to optimize the total number of cells employed in our simulations. This is important since the overall mesh quality could affect the accuracy of the results; on the other hand, increasing the total number of cells could affect the simulation runtimes. Therefore, simulations were performed with different mesh sizes to obtain grid independent results for the fluid flow. We progressively refined the grid (G1: 300 x 75; G2: 400 x 100 and G3: 450 x 110 mesh sizes) and calculated the difference in the obtained results. Fluid velocity changes by 0.54% when the mesh size is increased from G1 to G2. Further increase in the mesh size to G3 leads to a change in the velocity values only by 0.13%. Therefore, a mesh refinement beyond G2 increases the computational cost to a great extent (because the simulation time step decreases one order of magnitude) while it does not yield an appreciable improvement of the results.

2.2. Experimental validation of the theoretical model

The experiments for validating the model were performed using SU8 asymmetric and symmetric devices (Fig. 2 a)) with a rectangular cross-section of 200 µm x 200 µm (Microliquid). Two syringe pumps (Legato 210 infuse/withdraw syringe pump, Kd Scientific) and single syringes (Omnifix 5mL luer, BRAUN) were used to control the flow rate at each inlet independently. Tygon tubing (ø=0.8 mm) was employed for the fluidic connections, as seen in Fig. 2 b). Fluids with two different characteristics were pumped into the two inlets: a) Fluorescein sodium salt (($C_{20}H_{10}Na_2O_5$), (Scharlau (extra pure)) in water with a concentration of 60 $mg \cdot L^{-1}$ (Phase 1), and b) deionized water (Phase 2).

Fluorescence intensity (IF) caused by the presence of fluorescein in the fluid phases inside the microchip was detected on a microscope (Nikon SMZ18) equipped with a green fluorescence filter (light wavelengths of around 550 nm) and a Jenoptik ProgRes C5 camera (Fig. 2 c)). Images were taken using the ProgRes® CapturePro software (CapturePro V2.10.0.0). The quantification of flow patterns and diffusion phenomena was performed by analyzing the photographs taken by the camera with the software Image J (Version 1.50e, NIH, USA).

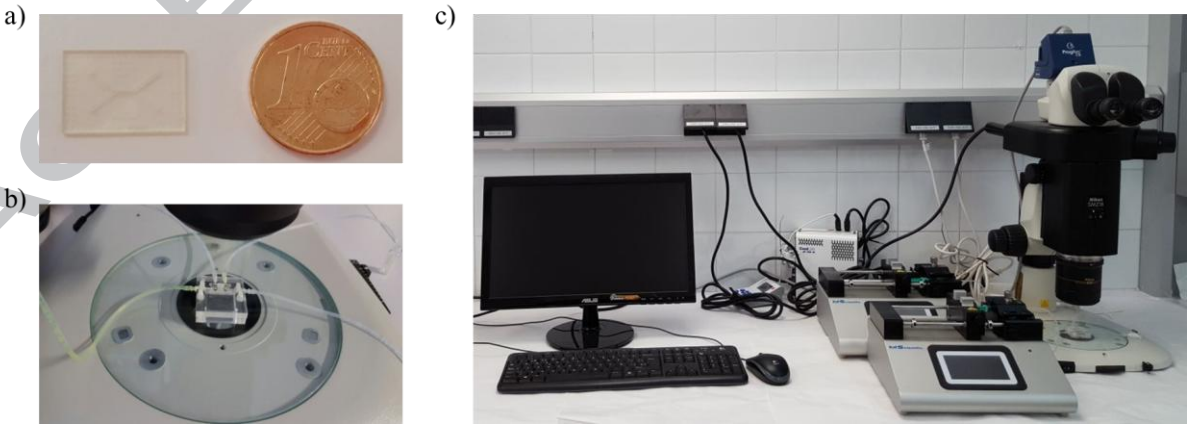

Fig. 2. Photograph of the experimental system. a) SU8 microfluidic device; b) Chip inserted in the holder showing the fluidic connections; c) Experimental setup showing the microscope and syringe pumps.

The co-flow of the phases under different experimental conditions was characterized for both symmetric and asymmetric devices. For the validation of the diffusion model, measurements of the evolution of IF as the fluids flow along the asymmetric channel (Configuration 1) were taken. The image analysis for this geometry was preceded by the sketch of a mesh in each photograph in order to analyze the same points in all images facilitating the comparison of results. Thus, the microchannel width was divided in different sections along the Z-axis, which are designated with letters (A, B, C, etc.). Besides, the chip length was divided in four parts (X-axis), corresponding to the quarter parts which are labelled with numbers from 1 to 5. This way, in each zone of the Z-axis, five measurements were done with Image J, as it is shown in Fig. 3.

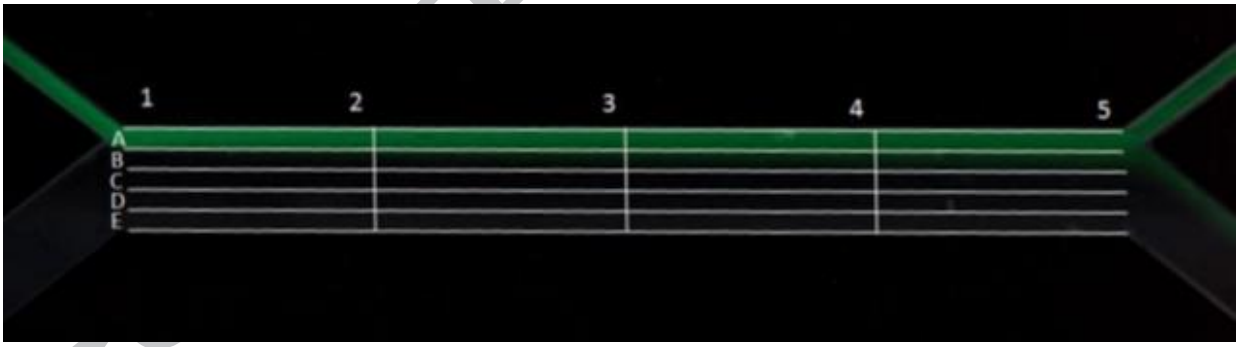

Fig. 3. Mesh sketch for image analysis and its application in an experimental image with the asymmetric chip (configuration 1).

The inhomogeneous illumination of the microscope and the possible contamination due to ambient light were compensated by considering the IF of the background. Besides, in order to

reduce the effects of the different illuminating conditions for each photograph and to make the results comparable, the IF was represented as a percentage (IF_{ij}/IF_{1A}) being i and j the zones considered in X- and Z-axis, respectively, and IF_{1A} corresponding to the IF at the system inlet.

3. RESULTS AND DISCUSSION

3.1. Flow patterns and phase separation studies

In this section, the flow patterns developed by both phases inside the different channels as a function of the average inlet velocities are analyzed, in order to examine the flow conditions that allow the complete separation of the fluids at the microdevice outlets. The volumetric fraction occupied by both phases inside the symmetric and both asymmetric devices under different velocity regimes (under which diffusion is considered negligible) is analyzed in Figs. 4 and 5, respectively. As seen in Fig. 4 a), where the prediction of the phase separation inside the symmetric device (α=1) is represented when both phases are introduced into the inlet of the device at the same mean velocity (set in this case at 1 $mm \cdot s^{-1}$, which corresponds to inlet flow rates of 72 $\mu L \cdot h^{-1}$), mixing at the outlets is not observed. Additionally, the experimental separation of the phases at the same velocity conditions inside the symmetric chip, shown in Fig. 4 b), is in good agreement with the computational model. In Fig. 4 c) the velocity vectors are represented for the previous conditions, showing the laminar regime developed inside the device with the fluid velocity vectors parallel to the x-axis due to the low Reynolds number (Re < 1).

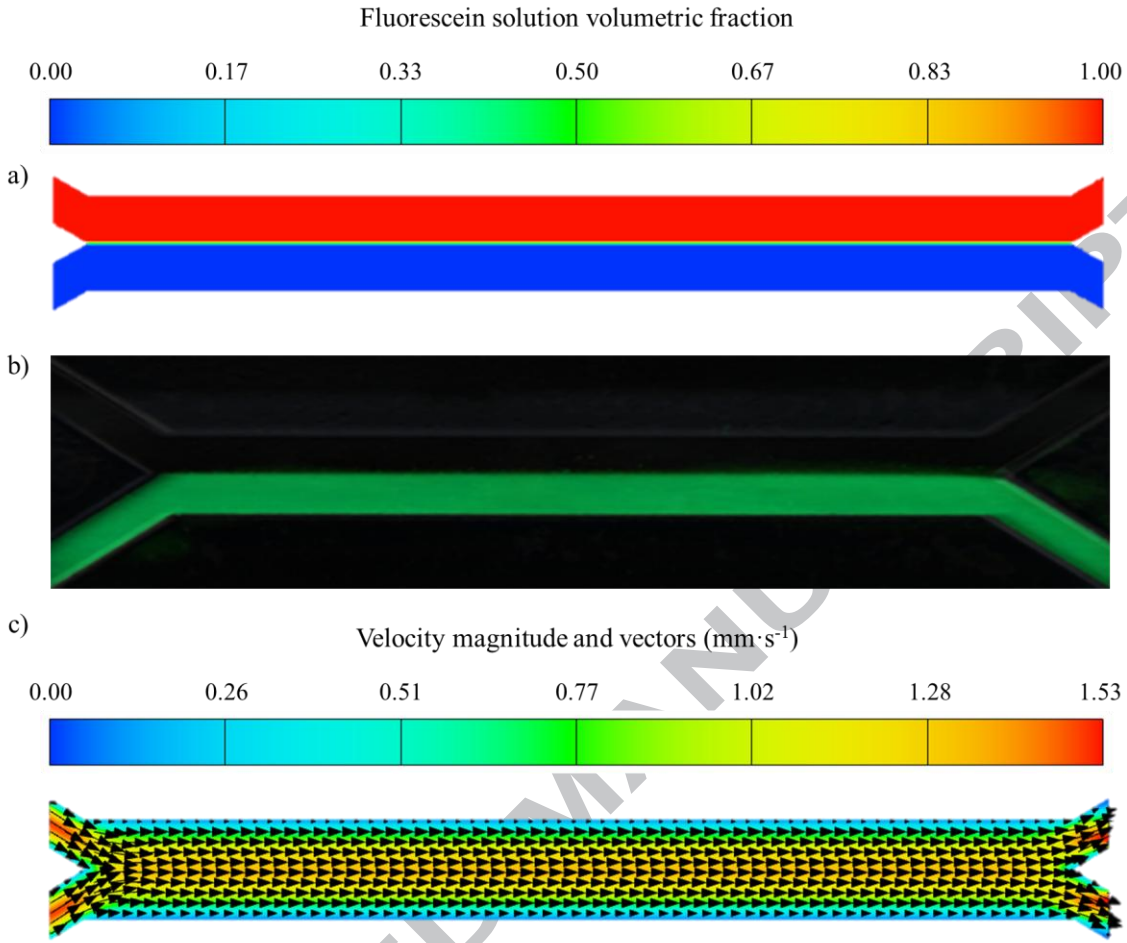

Fig. 4 a) Volumetric fraction of the fluorescein solution inside the symmetric chip for inlet phase's velocities equal to 1 $mm \cdot s^{-1}$ (72 $\mu L \cdot h^{-1}$); b) Experimental picture of the solution separation when the phases are pumped at the same flow rate inside the chip; c) Velocity magnitude and velocity vectors for the previous inlet velocity condition.

However, when α is different to 1 (asymmetric devices), phases do not separate at the outlets if they flow at the same velocity as shown in Fig. 5 a) for the configuration 1 of the asymmetric device. Although in both cases the phases flow in laminar regime (i.e. the fluid velocity vectors are parallel to the x-axis and the Reynolds number is below 1), the different pressure gradients created by each phase in the different branches of this geometry results in the penetration of the

fluorescein solution (red) to the lower outlet. In fact, when both fluids flow at the same velocity inside these geometries, such mixing effects at the outlets become even more pronounced as the difference between the height of the branches H_1 and H_2 increases. However, this behavior is not observed for the symmetric chip, since H_1 is set at the same value as H_2, as seen in Fig. 4. The complete separation of the fluid phases at the outlets in the asymmetric channels can be achieved by ensuring the same pressure drop at each phase throughout the length of the channel. By applying an approximation of the Hagen-Poiseuille law, it was demonstrated that this requirement is fulfilled when the value $\left(\frac{v_{mean,i}}{Ø_i^2}\right)_i$ for each phase "i" is the same, being $v_{mean,i}$ and $Ø_i$ the mean velocity of the phase "i" and the diameter of the branch where the phase "i" flows, respectively. Therefore, according to the branches dimensions in the configuration 1 of the asymmetric device, water (phase 2) should flow with a mean velocity of approximately 7.1 times higher than the mean velocity of the fluorescein phase to improve fluid separation at the microdevice outlets. Fig. 5 b) shows how the separation was enhanced at the outlets (the volume of phase 1 exiting the device through the lower outlet was reduced to almost 50%) when this criterion was applied, i.e. by setting inlet velocities of 2.8 $mm \cdot s^{-1}$ and 20.1 $mm \cdot s^{-1}$ for phase 1 and 2, respectively. This behavior has been experimentally validated, as seen in Fig. 5 c) which displays the experimental flow pattern of the phases flowing at the former velocity values and shows good agreement with the computational results. In Fig. 5 d) the velocity vectors are represented for the previous conditions, showing the laminar regime developed inside the microfluidic device due to the low Reynolds number. Following the same criterion, in Fig. 5 e), the phase separation for the configuration 2 of the asymmetric chip is shown. In this case, the complete separation can be achieved when the phase 1 flows with a mean velocity of approximately 7.1 times higher than the mean velocity of the phase 2 (water).

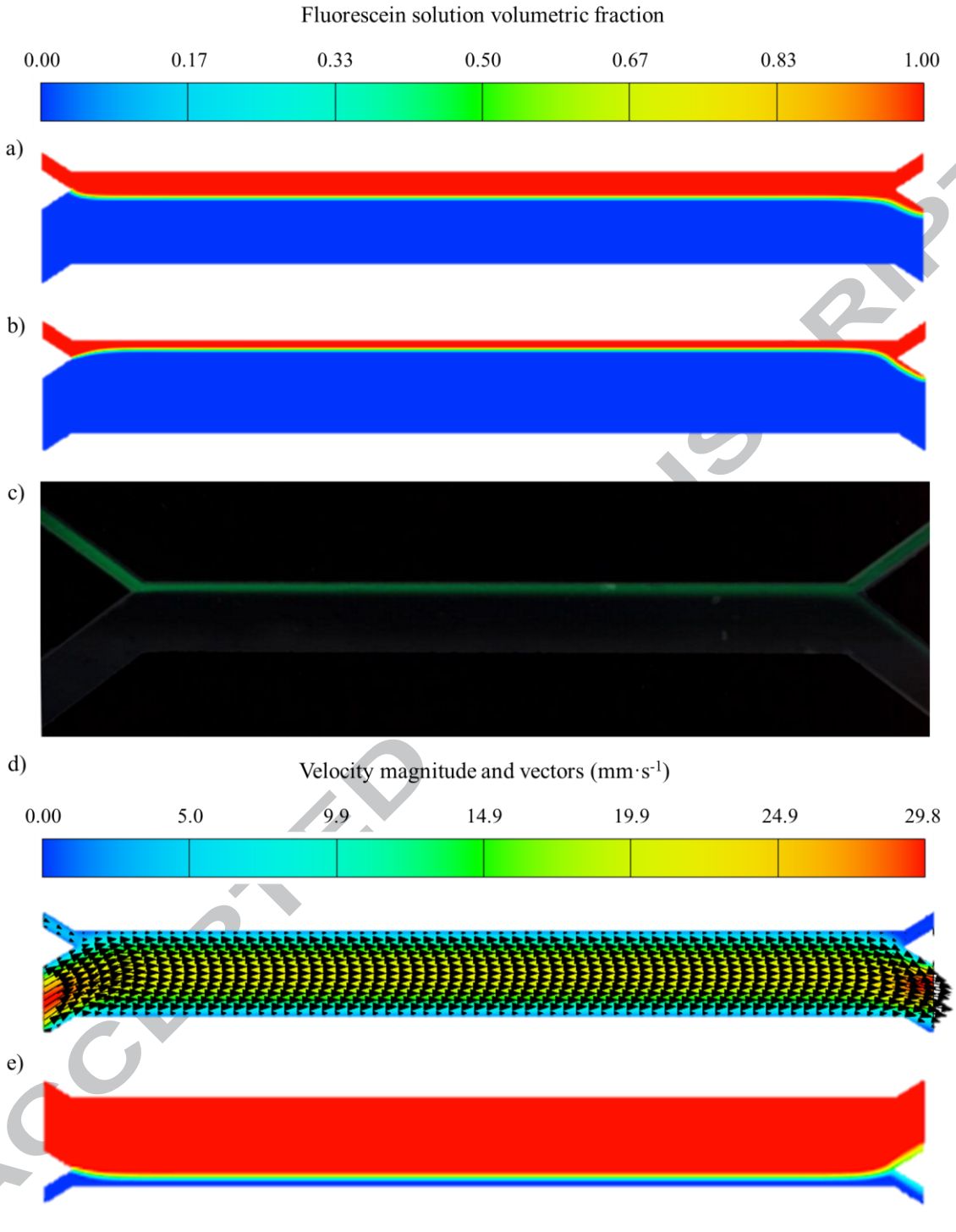

Fig. 5 Volumetric fraction of phase 1 inside the asymmetric device (configuration 1) under different phase's velocities at the inlets. a) $v_{fluorescein} = v_{water} = 1$ mm·s^{-1}; b) $v_{fluorescein} = 2.8$ mm·s^{-1} and $v_{water} = 20.1$ mm·s^{-1}; c) Experimental validation of the model for the velocity values

employed in case b); d) Velocity magnitude and velocity vectors for the previous velocity conditions; e)Volumetric fraction of the fluorescein solution inside the asymmetric chip (configuration 2) for phase's inlet velocities equal to 0.44 and 0.062 $mm \cdot s^{-1}$ for phases 1 and 2, respectively.

Nevertheless, it should be noted that when the properties of the fluid phases are different, this simplification is no longer valid because the pressure drop is influenced by the viscosity of each phase, as was previously observed by Kriel et al. [44]. Thus, the fluid properties of the solutions should be taken into account in order to set the same pressure drop in both branches of the channel when working with different fluids. Specifically, the value $\left(\frac{\eta_i v_{mean,i}}{\emptyset_i^2}\right)$ should be the same for each phase "i", where η_i is the viscosity of the phase i.

It should be noted that this approach is similar to the one presented by Foroozan Jahromi et al. for the separation of immiscible phases in Y-Y-shaped channels [45]. However, in the analysis reported by these authors, not only the Hagen Poiseuille law was employed but also the Bernoulli equation, and the altitudes of the outlet tubes were modified based on the pressure drop analysis to achieve phase separation at different flow rate values. In this case, the back-pressure at the end of the microchannel was neglected since the length of the outlet tubes was equal and short, and they were positioned at the same altitude. Instead, the flow rates were modified according to the pressure drop analysis.

3.2. Mass transfer analysis

In this section, the diffusion of fluorescein between the fluid phases is analyzed for the three selected geometries under the operation conditions that ensure the separation of phases. Specifically, the solute concentration profiles in each phase were examined for different values

of the parameter γ and the results were presented through the separation and concentration factors previously described. First, the diffusion time was calculated for each geometry and the velocity of phase 1 was fixed to calculate the residence time that provides a specific value of γ. Then, the velocity of phase 2 was calculated by employing the criterion developed in section 3.1. Besides, it should be remarked that, due to the fact that the mass transport of solute between phases is solely due to diffusion, its transport rate stops when both phases reach the equilibrium (the solute concentration is equal). Firstly, the theoretical model for diffusion was experimentally validated with the asymmetric microdevice (configuration 1) because of the higher velocity values that could be used with this geometry due to the low diffusion time; then the simulation results for the other geometries (symmetric and asymmetric in configuration 2) are discussed.

In Fig. 6, the concentration profiles of sodium fluorescein in the asymmetric device (α=0.25) obtained with the theoretical model and experimentally are represented for γ=4 and γ=0.1. It can be readily observed in Fig. 6 a) that for high values of γ, fluorescein keeps diffusing all along the length of the microdevice and the concentration of fluorescein that remains at the outlet is very low (only around 20% of the initial concentration). On the other hand, low γ values result in a poor diffusion of fluorescein; the solute is kept in the upper branch as advection dominates diffusion, as seen in Fig. 6 d). For this γ value, only 10% of the initial mass of fluorescein was transferred to the second phase by diffusion. This result can be perceived in Figs. 6 b, c), e) and f) where the experimental results have been compared for γ=4 and γ=0.1. Also, as seen in Fig. 6 c) where the straight section of the microchannel is zoomed in, a diffusional layer appears along the channel length, whereas for γ=0.1 (Fig. 6 f)) the interface between both fluids is clearly defined by a straight line. Furthermore, there is a good qualitative concordance between the results from model simulations and from the experiments.

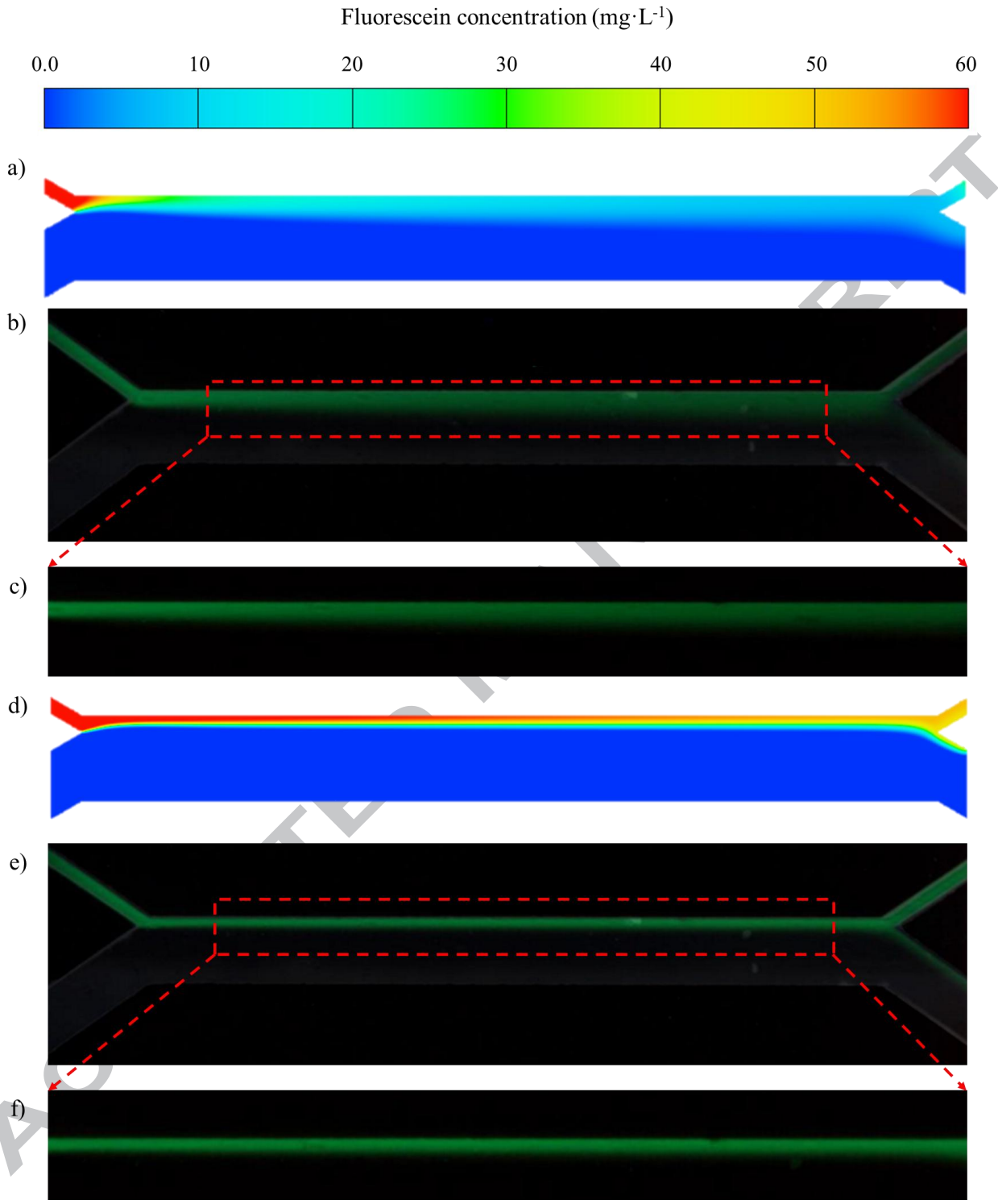

Fig. 6. Concentration of sodium fluorescein in the asymmetric chip (configuration 1) for γ=4: a) simulation results, b) and c) experimental results). γ=0.1: d) simulation results and e) and f) experimental results).

The diffusion phenomena have been quantified in Fig. 7, where the measurements of the IF expressed as a percentage (IF_{ij}/IF_{1A}, being i and j the zones considered in X- and Z-axis, respectively, and IF_{1A} corresponding to the IF at the system inlet) are represented for different values of the ratio γ. It can be easily observed that for high values of γ (Fig. 7 a) and b)), the IF detected in the zone where the fluorescein solution is expected to flow (zone A) decreases along the channel length as diffusion takes place, whereas in the adjacent zone (zone B), the IF follows the reverse trend (i.e. it increases along the axial direction of the channel). For instance, the IF decreases approximately 43% and 35% along the channel length in zone A for γ=4 and γ=2, respectively, as a consequence of the decrease in the fluorescein concentration in this zone due to diffusion. Besides, it can be noticed that the higher the γ-value, the higher the fluorescein detection in zone B which is in agreement with the behavior expected under these experimental conditions. Regarding the experiments in which γ values are lower than 1 (Fig. 7 c) and d)), the IF observed in zone A is maintained constant as the solution flows to the system outlet, as unfavorable mass transfer conditions have been considered. This means that diffusion phenomena between adjacent fluid layers are greatly minimized as there is no fluorescein (or the amount is negligible) in the contiguous zones to zone A (i.e. zone B). Finally, the diffusion phenomenon has been verified by the accomplishment of the IF balance for each measurement (i.e. the sum of the IF detected in each of the measurements in the z-axis for a fixed x value must be equal to the one corresponding to the inlet IF_{1A}). The graphical representation of the IF balance is shown in Figure 7 e) and f) for γ= 4 and γ= 2, respectively. It should be noted that the global IF reported for each X-axis measurement (i index) is approximately equal to the value corresponding to the inlet (IF_{1A}). The situations in which the balance is not completely fulfilled might be due to the inhomogeneous illumination conditions inside the device and the

experimental error. However, in almost all cases the IF balance is practically fulfilled depicting a satisfactory global value with an error lower than 15%.

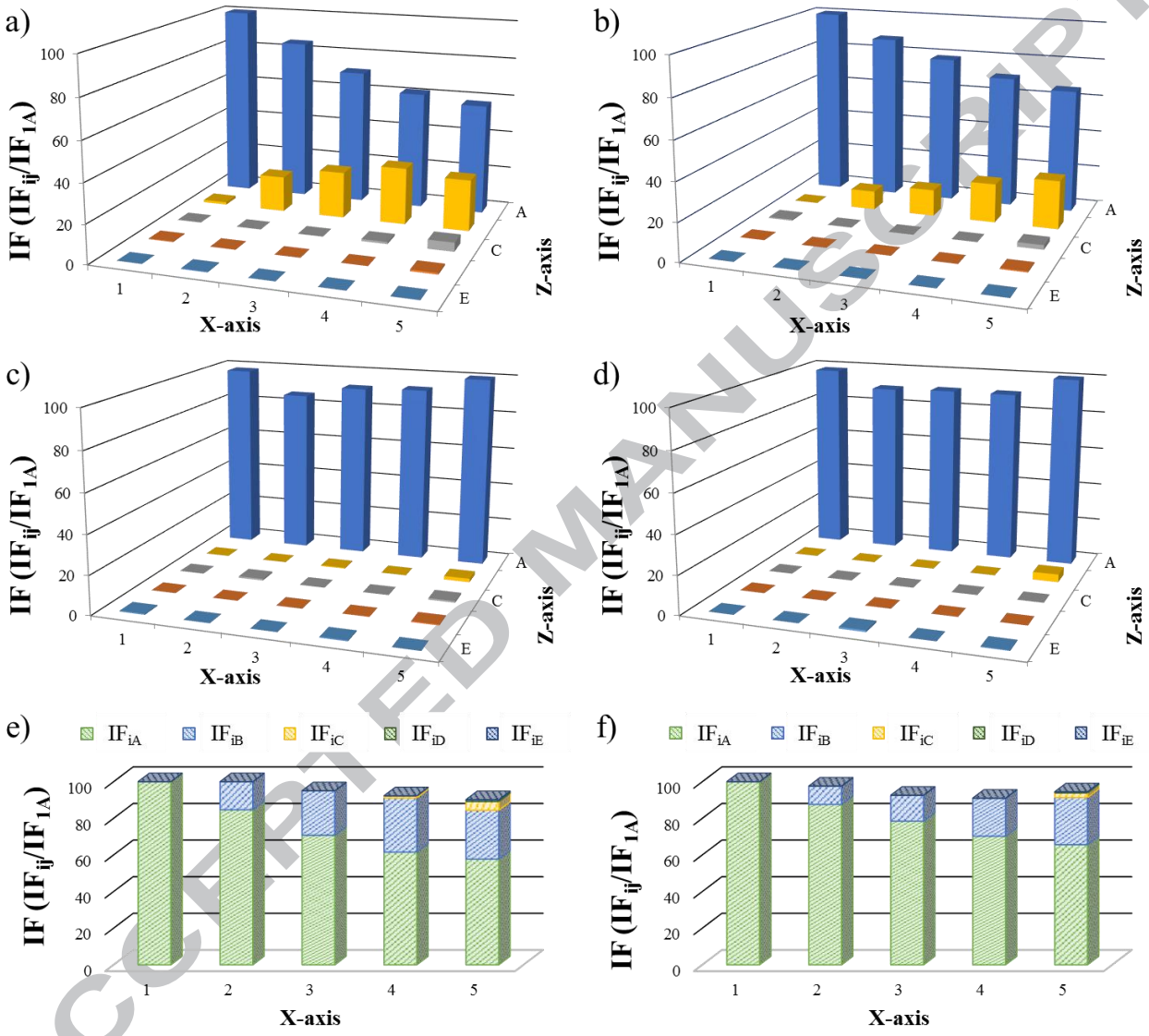

Fig. 7. IF in the different zones (from A to E) of the channel for different γ-values. a) γ=4; b) γ=2; c) γ =0.25; d) γ=0.1; e) IF balance fulfillment for γ=4; f) IF balance fulfillment for γ=2.

Once the results obtained with the theoretical model have been contrasted against the experimental data and good agreement between them has been relatively found, the comparison of the diffusion results between the three geometries is presented. Fig. 8 a) represents the separation factor as a function of γ for the three studied geometries in which different α ratios are employed (0.25 corresponds to the asymmetric device in its configuration 1, 1 represents the symmetric device and 4 is the configuration 2 of the asymmetric chip). On the other hand, Fig. 8 b) shows the influence of γ on the concentration factor. It can be seen in this figure that as γ increases, both the separation and concentration factors increase, which means that higher amount of solute is being removed from phase 1 and recovered in phase 2. However, the separation factor increases as the volumetric ratio α decreases, whereas the concentration factor follows the reverse trend.

For example, when $\alpha=1$, the separation factor is limited to 50% for high γ values, i.e. when the concentration of the solute is the same in both fluid phases. Therefore, maximum concentration in phase 2 is also limited to 50% of the initial concentration in phase 1 when $\gamma\geq1$. This effect has been reported in previous studies [26]. However, this is not observed when the ratio α is different from 1. In fact, when α is lower than 1 (asymmetric devices in the configuration 1), the separation factor is always higher than 50% when $\gamma\geq1$. As seen in Fig. 8 a), the separation factor varies from 60 to 80% when γ increases from 1 to 4. On the other hand, the separation factor reported by devices with α ratios higher than 1 (asymmetric devices in the configuration 2) is negligible for all the γ values tested (in this case, it varies from 2.7 to 4.3% as γ increases from 0.1 to 4). Thus, this type of devices are not practical for those applications where high removal of the solutes by diffusion are required.

Nonetheless, the concentration factor which relates the concentration of the solute at the outlet of phase 2 follows the opposite trend. In these cases, the higher the α ratio, the higher the concentration factor observed. For instance, and due to the different volumes of the donor and the receiving phase, when α goes down to 0.25, the concentration reported at the outlet of phase 2 is practically negligible, because of the high volume of the receiving phase. In this case, it is kept constant at values of around 7% for the range of γ under study. On the contrary, with asymmetric devices in their configuration 2 (α >> 1), high concentration of the solute in the phase 2 is reported (93-96%) while the dilution of phase 1 is negligible at the same time due to the low volume of the receiving phase with this configuration.

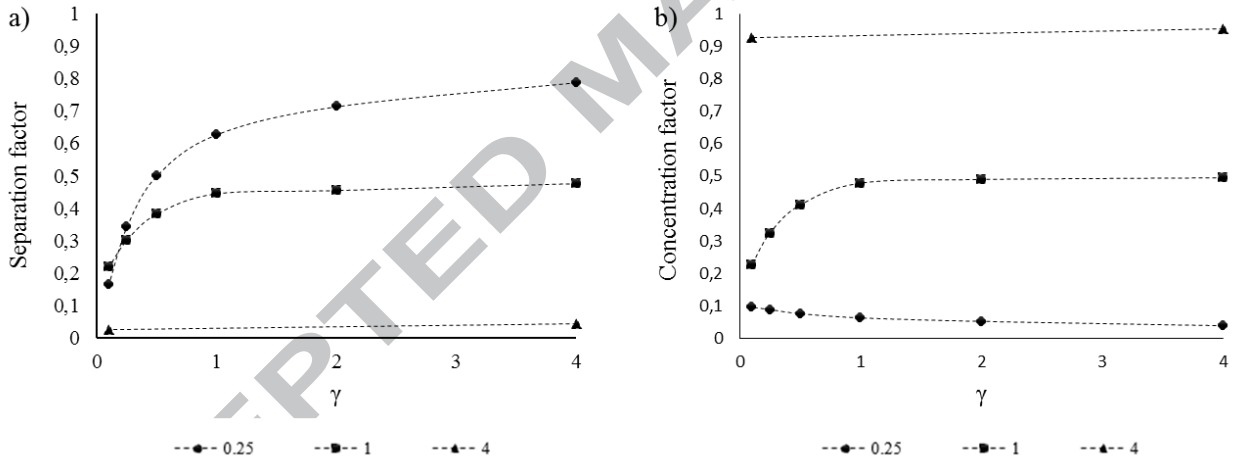

Fig. 8. a) Separation factor and b) Concentration factor as a function of γ for the α ratios under study (α equal to 0.25 and 4 are the asymmetric devices for the configuration 1 and 2, respectively, whereas 1 represent the symmetric device).

Finally, the analysis of the fluorescein mass flows at both outlets as a function of γ are presented in Fig. 9, where the results are compared for the chips with α ratios of 0.25 and 1 (results for the

device with a α ratio of 4 are not discussed due to the low mass flows obtained). As it can be observed in Fig. 9, the solute mass flow increases as γ diminishes for both geometries due to the increased fluid inlet flowrates employed for low γ values. Additionally, it should be noted that the fluorescein mass flow of both phases decreases as α increases. This effect is caused by the high diffusion times (proportional to H_1^2) for higher α values and thus, the low fluid flowrate employed for the same γ. This is why the mass flow results for the configuration with a α ratio of 4 are almost negligible (at least two orders of magnitude lower than the values corresponding to the rest of geometries).

Furthermore, the mass flows for both phases are the same when $\gamma \geq 1$ for the symmetric device, since at these γ values the concentration reported by both phases is the same (as well as the flowrates of both fluid phases employed for this device), as shown in Fig. 9. However, as γ diminishes, the solute mass flow of the phase 1 increases because of the greater concentration in this phase when low residence times are applied.

On the other hand, this behavior is not observed when α is lower than 1. For the configuration 1 of the asymmetric device, higher mass flows are observed in phase 2 for all the γ values analyzed. In this case, phase 1 flows with much lower flowrate than phase 2 in order to ensure the same pressure drop for both phases along the channel length and avoid phase mixing at the outlets (as developed in section 3.1). Since the solute mass flow is the product between the concentration and the fluid flowrate, the observed results are highly dependent on the higher fluid flowrate of phase 2, reaching solute mass flows values as high as 33.7 $\mu g \cdot h^{-1}$ for phase 2, as seen in Fig. 9.

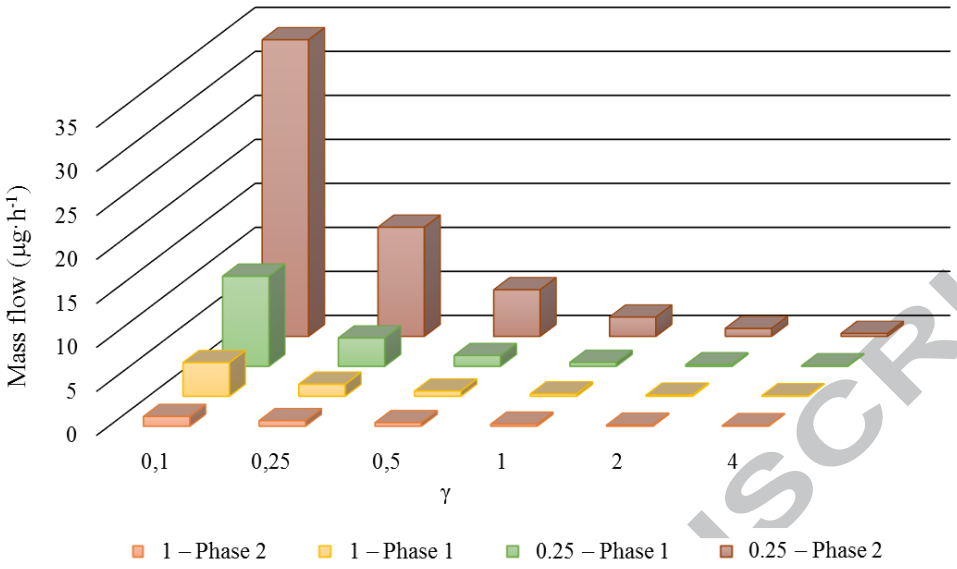

Fig. 9. Solute mass flow at both outlets for the symmetric (α=1) and asymmetric device in the configuration 1 (α=0.25).

4. CONCLUSIONS

Microfluidics has emerged as a novel technology able to integrate physical and chemical processes to achieve effective separations at a low cost within a small volume. Accordingly, multiple applications in analytical chemistry, biochemistry, pharmacy, etc. have been developed in recent years due to the advantages of the microscale (i.e. large area-to-volume ratio, short diffusion distances/times, etc.). Nevertheless, for two fluid phases flowing through microdevices, the progress in this technology and the deployment of new separation applications rely on the ability to understand the coupled influence of fluid dynamics and the solute mass transfer rate from the donor to the receiving phase in the separation and concentration factors reached in the microdevice.

In this work, we deeply analyze the influence of operation and geometric variables in the performance of microfluidic separation devices with two homogeneous fluid phases. The flow

patterns of miscible fluids inside Y-Y shaped microfluidic devices (asymmetric and symmetric channel geometries) have been studied both experimentally and theoretically, as well as the diffusive transport of a model component (fluorescein) from a donor phase to a receiving phase. We have demonstrated that the phase separation inside the symmetric device can be achieved when both phases flow at the same mean velocity, however, under these circumstances mixing at the outlets is observed for the asymmetric devices. Nevertheless, by ensuring the same pressure drop for both solutions (a function of phase velocity, fluid properties and geometrical characteristics of the channel) phase separation inside the asymmetric channels can be improved. Furthermore, the rate of molecular diffusion was analyzed for the first time in both symmetric and asymmetric devices as a function of γ (ratio between the residence time of the donor phase in the chip and the diffusion time of the solute). Results showed that different separation factors and solute mass flows at the outlet of both phases were obtained for the same γ values when varying the volumetric ratio between phases α (determined in this work through different channel configurations). In fact, α ratios lower than 1 (asymmetric devices with configuration "1") could be used for applications where high separation factors and high solute mass flows are required, whereas the configuration "2" (α ratios higher than 1) demonstrated to be the best geometry for those processes where high concentration factors are needed. Finally, when α is equal to 1 (symmetric devices), the concentration and solute mass flows are limited by the solute concentration equilibrium between the fluid phases for high γ values. Therefore, this analysis provides the optimum fluid dynamic conditions (γ values) and geometry configuration (α ratio) for any specific application.

ACKNOWLEDGEMENTS

Financial support from the Spanish Ministry of Economy and Competitiveness under the projects CTQ2015-72364-EXP/AEI and CTQ2015-66078-R (MINECO/FEDER) is gratefully acknowledged. Jenifer Gómez-Pastora also thanks the FPI postgraduate research grant (BES-2013-064415). Cristina González-Fernández thanks the Concepción Arenal postgraduate research grant from the University of Cantabria.

REFERENCES

[1] P.N. Nge, C.I. Rogers, A.T. Woolley, Advances in microfluidic materials, functions, integration, and applications, Chem. Rev. 113 (2013) 2550–2583.

[2] N. Pamme, On-chip bioanalysis with magnetic particles, Curr. Opin. Chem. Biol. 16 (2012) 436–443.

[3] W.K.T. Coltro, C.M. Cheng, E. Carrilho, D.P. de Jesus, Recent advances in low cost microfluidic platforms for diagnostic applications, Electrophoresis 35 (2014) 2309–2324.

[4] Z. Zhang, L. Yu, L. Xu, X. Hu, P. Li, Q. Zhang, X. Ding, X. Feng, Biotoxin sensing in food and environment via microchip, Electrophoresis 35 (2014) 1547–1559.

[5] A.L. Dessimoz, L. Cavin, A. Renken, L. Kiwi-Minsker, Liquid–liquid two-phase flow patterns and mass transfer characteristics in rectangular glass microreactors, Chem. Eng. Sci. 63 (2008) 4035–4044.

[6] A. Sahu, A.B. Vir, L.N.S. Molleti, S. Ramji, S. Pushpavanam, Comparison of liquid-liquid extraction in batch systems and micro-channels, Chem. Eng. Process. Process Intenfic. 104 (2016) 190–200.

[7] N. Assmann, A. Ladosz, P.R. von Rohr, Continuous Micro Liquid-Liquid Extraction, Chem. Eng. Technol. 36 (2013) 921–936.

[8] T. Han, L. Zhang, H. Xu, J. Xuan, Factory-on-chip: Modularised microfluidic reactors for continuous mass production of functional materials, Chem. Eng. J. 326 (2017) 765–773.

[9] N. Di Miceli Raimondi, L. Prat, C. Gourdon, J. Tasselli, Experiments of mass transfer with liquid–liquid slug flow in square microchannels, Chem. Eng. Sci. 105 (2014) 169–178.

[10] N. Milozic, M. Lubej, M. Lakner, P. Znidarsic-Plazl, I. Plazl, Theoretical and experimental study of enzyme kinetics in a microreactor system with surface-immobilized biocatalyst, Chem. Eng. J. 313 (2017) 374–381.

[11] J. Gómez-Pastora, X. Xue, I.H. Karampelas, E. Bringas, E.P. Furlani, I. Ortiz, Analysis of separators for magnetic beads recovery: from large systems to multifunctional microdevices, Sep. Purif. Technol. 172 (2017) 16–31.

[12] R. Monosik, L. Angnes, Utilisation of micro- and nanoscaled materials in microfluidic analytical devices, Microchem. J. 119 (2015) 159–168.

[13] D. Liu, K. Wang, Y. Wang, Y. Wang, G. Luo, A simple online phase separator for the microfluidic mass transfer studies, Chem. Eng. J. 325 (2017) 342–349.

[14] A.Q. Alorabi, M.D. Tarn, J. Gómez-Pastora, E. Bringas, I. Ortiz, V.N. Paunov, N. Pamme, On-chip polyelectrolyte coating onto magnetic droplets – Towards continuous flow assembly of drug delivery capsules, Lab Chip (2017), http://dx.doi.org/10.1039/C7LC00918F.

[15] S. Hossain, I. Lee, S.M. Kim, K.Y. Kim, A micromixer with two-layer serpentine crossing channels having excellent mixing performance at low Reynolds numbers, Chem. Eng. J. 327 (2017) 268–277.

[16] M.D. Tarn, M.J. Lopez-Martinez, N. Pamme, On-chip processing of particles and cells via multilaminar flow streams, Anal. Bioanal. Chem. 406 (2014) 139–161.

[17] A.A.Yagodnitsyna, A.V. Kovalev, A.V. Bilsky, Flow patterns of immiscible liquid-liquid flow in a rectangular microchannel with T-junction, Chem. Eng. J. 303 (2016) 547–554.

[18] R. Raj, N. Mathur, V.V. Buwa, Numerical simulations of liquid-liquid flows in microchannels, Ind. Eng. Chem. Res. 49 (2010) 10606–10614.

[19] T. Fu, L. Wei, C. Zhu, Y. Ma, Flow patterns of liquid–liquid two-phase flow in non-Newtonian fluids in rectangular microchannels, Chem. Eng. Process. Process Intensif. 91 (2015) 114–120.

[20] P. Plouffe, D.M. Roberge, A. Macchi, Liquid–liquid flow regimes and mass transfer in various micro-reactors, Chem. Eng. J. 300 (2016) 9–19.

[21] J. Atencia, D.J. Beebe, Controlled microfluidic interfaces, Nature 437 (2005) 648–655.

[22] D.M. Anderson, G.B. McFadden, A.A. Wheeler, Diffuse-interface methods in fluid mechanics, Annu. Rev. Fluid Mech. 30 (1998) 139–165.

[23] R.F. Ismagilov, A.D. Stroock, P.J.A. Kenis, G. Whitesides, H.A. Stone, Experimental and theoretical scaling laws for transverse diffusive broadening in two-phase laminar flows in microchannels, Appl. Phys. Lett. 76 (2000) 2376–2378.

[24] Y. Zhou, Y. Wang, Q. Lin, A microfluidic device for continuous-flow magnetically controlled capture and isolation of microparticles, J Microelectromech. Syst. 19 (2010) 743–751.

[25] M. Surmeian, A. Hibara, M. Slyadnev, K. Uchiyama, H. Hisamoto, T. Kitamori, Distribution of methyl red on the water-organic liquid interface in a microchannel, Anal. Lett. 34 (2001) 1421–1429.

[26] D. Ciceri, J.M. Perera, G.W. Stevens, A study of molecular diffusion across a water/oil interface in a Y–Y shaped microfluidic device, Microfluid. Nanofluid. 11 (2011) 593–600.

[27] J. Gómez-Pastora, I.H. Karampelas, X. Xue, E. Bringas, E.P. Furlani, I. Ortiz, Magnetic bead separation from flowing blood in a two-phase continuous-flow magnetophoretic microdevice: theoretical analysis through computational fluid dynamics simulation, J. Phys. Chem. C 121 (2017) 7466–7477.

[28] C.W. Yung, J. Fiering, A.J. Mueller, D.E. Ingber, Micromagnetic-microfluidic blood cleansing device, Lab Chip 9 (2009) 1171–1177.

[29] G. Helle, C. Mariet, G. Cote, Liquid-liquid two-phase microflow patterns and mass transfer of radionuclides, 9th IEEE International Conference on Nano/Micro Engineered and Molecular Systems, IEEE-NEMS 6908781 (2014) 157–162.

[30] J.B. Salmon, A. Ajdari, Transverse transport of solutes between co-flowing pressure-driven streams for microfluidic studies of diffusion/reaction processes, J. Appl. Phys. 101 (2007) 074902.

[31] J. Dambrine, B. Geraud, J.B. Salmon, Interdiffusion of liquids of different viscosities in a microchannel, New J. Phys. 11 (2009) (075015).

[32] T. Hotta, S. Nii, T. Yajima, F. Kawaizumi, Mass transfer characteristics of a microchannel device of split-flow type, Chem. Eng. Technol. 30 (2007) 208–213.

[33] S. Hardt, T. Hahn, Microfluidics with aqueous two-phase systems, Lab Chip 12 (2012) 434–442.

[34] H. Bruus, Acoustofluidics 10: scaling laws in acoustophoresis, Lab Chip 12 (2012) 1578–1586.

[35] M. Sattari-Najafabadi, M.N. Esfahany, Z. Wu, B. Sundén, Hydrodynamics and mass transfer in liquid-liquid non-circular microchannels: comparison of two aspect ratios and three junction structures, Chem. Eng. J. 322 (2017) 328–338.

[36] D. Tsaoulidis, P. Angeli, Effect of channel size on mass transfer during liquid–liquid plug flow in small scale extractors, Chem. Eng. J. 262 (2015) 785–793.

[37] M. Sattari-Najafabadi, M.N. Esfahany, Z. Wu, B. Sundén, The effect of the size of square microchannels on hydrodynamics and mass transfer during liquid-liquid slug flow, AIChE J. 63 (2017) 5019–5028.

[38] M.N. Kashid, A. Renken, L. Kiwi-Minsker, Influence of flow regime on mass transfer in different types of microchannels, Ind. Eng. Chem. Res. 50 (2011) 6906–6914.

[39] G. Liu, K. Wang, Y. Lu, G. Luo, Liquid–liquid microflows and mass transfer performance in slit-like microchannels, Chem. Eng. J. 258 (2014) 34–42.

[40] C.W. Hirt, B.D. Nichols, Volume of Fluid (VOF) method for the dynamics of free boundaries, J. Comput. Phys. 39 (1981) 201–225.

[41] H. Bruus, Theoretical Microfluidics, Oxford University Press, New York, 2008.

[42] C.T. Culbertson, S.C. Jacobson, J.M. Ramsey, Diffusion coefficient measurements in microfluidic devices, Talanta 56 (2002) 365–373.

[43] S. Erdogan, M. Wörner, Influence of channel cross-sectional shape on diffusion-free residence time distribution in fully developed laminar newtonian flow, Chem. Eng. J. 227 (2013) 158–165.

[44] F.H. Kriel, S. Woollam, R.J. Gordon, R.A. Grant, C. Priest, Numbering‐up Y–Y microfluidic chips for higher‐throughput solvent extraction of platinum(IV) chloride, Microfluid. Nanofluid. 20 (2016) 138–144.

[45] P.F. Jahromi, J. Karimi-Sabet, Y. Amini, H. Fadaei, Pressure-driven liquid-liquid separation in Y-shaped microfluidic junctions, Chem. Eng. J. 328 (2017) 1075–1086.

- Miscible liquid-liquid flow patterns in different microchannels are presented.
- Mass transfer of a model component between homogeneous flowing phases is analyzed.
- Evaluation of the residence and diffusion times ratio (γ) on mass transfer.
- The influence of the volumetric ratio between phases (α) is studied.
- Separation and concentration factors for different γ and α values are calculated.